AUTOMATIC EXCLUSION OF SURFACE DEFORMATION IN INSAR DEM GENERATION USING DIFFERENTIAL RADAR INTERFEROMETRY

Jung Hum Yu[1] and Linlin Ge

School of Surveying and Spatial Information Systems, University of New South Wales, Australia
[1]Jung.yu@student.unsw.edu.au

1. INTRODUCTION

Digital Elevation Models (DEMs) are an important source of topographical data for many scientific and engineering applications such as hydrological and geological studies, infrastructure planning and environmental impact investigations. Where topographical data is unavailable, typically DEMs from remotely sensed data can be generated and used as the main source of information. Repeat-pass satellite SAR interferometry (InSAR) is a one method for low-cost, relatively precise and wide-coverage surface DEM generation. InSAR is a technique for extracting three-dimensional terrain information from the phase "interferograms" of two SAR data images [1]. In InSAR DEM processing one major assumption for interferogram calculation is that if the imaging interval is sufficiently short, the total interferogram has no deformation phase signal. However, repeat cycles of satellite SAR systems are in the range of 11~46 days. This interval is long enough time for ground deformation caused by non-natural effects to become evident. The ground deformation is not completely removed from the interferometric fringes of the InSAR because any ground deformation that has taken place is simply ignored. Differential (DInSAR) is a cost-effective technique for surface displacement mapping. Basic processing requirements are the same as in the case of InSAR processing. DInSAR processing requires the removal of interferometric phase that are contributed to by the topography, hence isolating the ground displacement component [3, 5]. The authors propose a combination method that generates a mask of the ground deformation area during DInSAR processing, and then improves the accuracy of InSAR DEM generation by removing ground deformation.

2. DEM GENERATION USING InSAR AND DInSAR

InSAR combines complex images recorded either by two satellite antennas at different locations at the same time, or with the same antenna at two different times of satellite overpass. The phase difference information between the SAR images is used to measure precise changes in the range or distance from the antenna locations to the corresponding point in an image pair [7]. The differential phase from two independent SAR images of the same ground pixel target contains useful 3D terrain information. The elevation information is obtained from the interferogram by "unwrapping" the interferometric phases. The interferometric phase can be written as:

$$\phi_{InSAR}=\phi_{flat}+\phi_{topo}+\phi_{defo}+\phi_{atm}+\phi_{noi} \quad (1)$$

where ϕ_{InSAR} is the interferometric phase, ϕ_{flat} is the so-called "flat earth" phase, ϕ_{topo} is the topographic phase, ϕ_{defo} is the deformation phase, ϕ_{atm} is the atmospheric delay phase and ϕ_{noi} is the noise. The "flat earth" phase ϕ_{flat} and noise ϕ_{noi} can be removed by using orbit information corrections and applying an interferogram filtering method. When the imaging interval is sufficiently short, it can be assumed that there is no deformation phase ϕ_{defo}. If the atmospheric delay phase ϕ_{atm} can be ignored:

$$\phi_{InSAR} = \phi_{topo} \tag{2}$$

The DEM is obtained by "unwrapping" the phase ϕ and converting the phase to a height quantity for the pixel, and then geo-coding the pixel [1].

DInSAR measures ground deformation using repeat-pass interferometry with an accuracy and spatial measurement density which is unprecedented. In the equation (1), topographical fringes ϕ_{topo} are calculated from simulated fringes which were generated using an external DEM, and subtracted from the original interferogram. Only the fringes representing surface displacements remain [4]:

$$\phi_{DInSAR} = \phi_{defo} \tag{3}$$

3. METHODOLOGY

In this paper an external DEM is used to generate the topographic phase which is then subtracted from the interferogram. Interferometric processing requires a comparatively short temporal baseline between image acquisitions in order to ensure maximum coherence [2]. The DInSAR technique is based on the use of two SAR images and the differential interferogram, as the name implies, is the difference of two interferograms [6]. In DInSAR processing the areas of ground deformation are presented by repeat cycle fringes between $-\pi$ to π while other non-deforming areas have a common phase value. In other words, the ground deformation fringes are distinct from stable ground phase, and is in fact an important distinguishing characteristic of deformation areas. The deformation mask step is: 1) selection of a specific phase value using the threshold method (each DInSAR has different a value), 2) expansion of selected area (to cover the deformation area), 3) exclusion of noisy pixel (unexpected area), and 4) identification of deformation area and extraction of fringes.

4. EXPERIMENTAL RESULT

The test site considered is the Appin area in the state of New South Wales, Australia. This research used Advanced Land Observing Satellite SAR images (acquisition dates: 14/11/07, 30/12/07, and 14/02/08) to generate the ground subsidence map and the DEM. In the DInSAR processing, the master and slave images were selected in the same order as InSAR DEM generation processing. In the test area, the ground subsidence corresponded to two underground mining areas. Figure 1 is the resulting ground subsidence map from DInSAR processing and InSAR-generated DEM and deformation mask. The ground deformation area is

identified from the DInSAR result. Comparing the InSAR-generated DEM with the DInSAR-derived deformation map, the ground deformation area appears to correctly overlap with the DEM height error area.

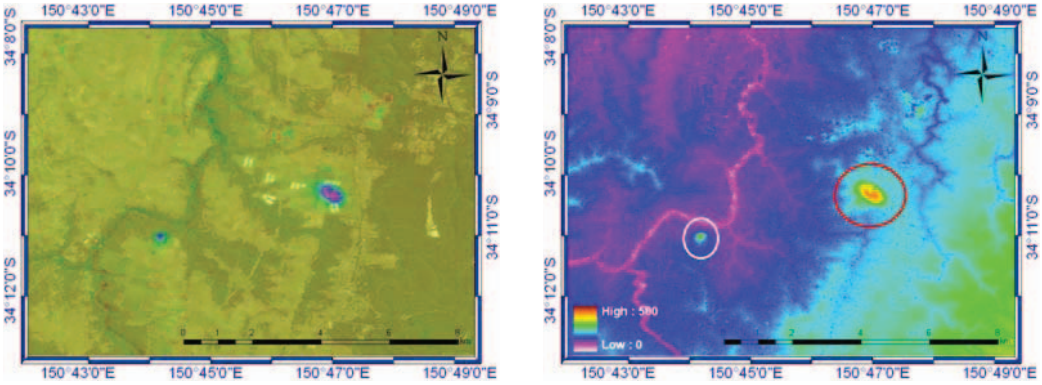

Fig. 1. DInSAR subsidence map, deformation mask and InSAR-generated DEM in the Appin test site.

The specific phase value (deformation area), to distinguish the deforming area from the non-deforming area, is determined. The deformation mask is allowed to grow based on the candidate pixels, using 16-neighbourhood windows. In particular, the mask growing processing occurs from two different image directions because the mask shape patterns are affected by the image processing direction. After calculating the mask area, the extended mask is filtered to remove the noise (detection error). The deformation area exclusion is performed at the interferogram level in InSAR processing. The deforming area is extracted using the deformation mask, hence the deformation mask and InSAR interferogram have to have the same image coordinate system and size. (The mask provides the deformation pixel location and this location is applied to the interferogram of InSAR.) Removed deformation area is replaced and interpolated by surrounding pixel values and external DEM information. After deformation exclusion processing, the subsequent processing steps are as per the standard InSAR DEM processing. Figure 2 is the InSAR-generated DEM and the reprocessed InSAR-generated DEM. Height errors which are affected by ground deformation have been removed.

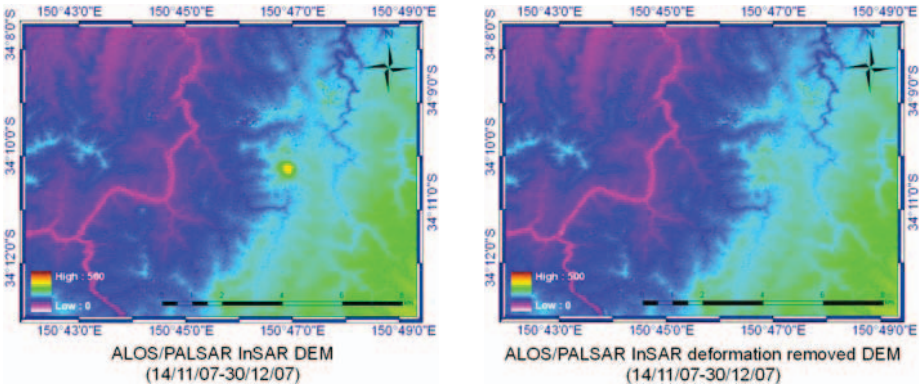

Fig. 2. InSAR-generated DEM (left) and DEM with deformation removal (right) (14/11/07-14/02/08).

5. CONCLUDING REMARKS

Two ALOS/PALSAR image pairs have been used for InSAR DEM generation. These image pairs also have been used for DInSAR processing to detect areas of ground subsidence. In this paper, the location of ground subsidence is important information used to remove the terrain elevation errors in an InSAR-derived DEM. The space-borne SAR systems have revisit cycles which are long enough for the terrain conditions to change.

Therefore, ground deformation should be excluded from InSAR DEM generation. Ground deformation areas are detected using the DInSAR method. The candidate pixels for deformation detection are selected using a threshold phase value and is the area is extended by the use of a searching window. The detected area is removed from InSAR processing and interpolated using a combination of the reference elevation value and surrounding elevation values. The elevation error due to ground deformation is removed and the regenerated DEM accuracy is improved.

6. REFERENCES

[1] A. Ferretti, C. Prati, and F. Rocca, "Permanent scatterers in SAR interferometry", *IEEE Transactions on Geoscience & Remote Sensing*, vol. 39(1), pp. 8-20, 2001.

[2] D.T. Sandwell, D. Myer, R. Mellors, M. Shimada, B. Brooks, and J Foster, "Accuracy and resolution of ALOS interferometry: vector deformation maps of the Father's Day intrusion at Kilauea", *IEEE Transactions on Geoscience & Remote Sensing*, vol. 46(11), pp. 3524-3534, 2008.

[3] H.C. Chang, L. Ge, A.H.M. Ng, C. Rizos, H. Wang, and M. Omura, "Combination of multiple repeat orbits of ENVISAT for mine deformation monitoring", *IAG Symposia Series*, vol. 133, pp.631-638, 2008.

[4] L. Ge, H.C. Chang, and C. Rizos, "Mine subsidence monitoring using multi-source satellite SAR images", *Photogrammetric Engineering & Remote Sensing*, vol. 73(3), pp. 259-266, 2007.

[5] L. Ge, K. Zhang, A.H.M. Ng, Y. Dong, H.C. Chang, and C. Rizos, "Preliminary results of satellite radar interferometry for the co-seismic deformation of the 12 May 2008 Ms 8.0 Wenchuan earthquake", *Journal of Geographic Information Science*, vol. 14(1), pp. 12-19, 2008.

[6] P. Berardino, G. Fornaro, R. Lanari, and E. Sansosti, "A new algorithm for surface deformation monitoring based on small baseline differential SAR interferograms", *IEEE Transactions on Geoscience and Remote Sensing*, vol. 40(11), pp. 2375-2383, 2002.

[7] T. Toutin, and L. Gray, "State-of-the-art of elevation extraction from satellite SAR data", *ISPRS Journal of Photogrammetry & Remote Sensing*, vol. 55(1), pp. 13-33, 2000.